ANTIOXIDANTS & REDOX SIGNALING
Volume 14, Number 6, 2011

DOI: 10.1089/ars.2010.3297

ORIGINAL RESEARCH COMMUNICATION

Brain Nitric Oxide Inactivation Is Governed by the Vasculature

Ricardo M. Santos,[1] Cátia F. Lourenço,[1] François Pomerleau,[2] Peter Huettl,[2] Greg A. Gerhardt,[2] João Laranjinha,[1,3] and Rui M. Barbosa[1,3]

Abstract

The mechanisms underlying nitric oxide (•NO) synthesis and inactivation in the brain are essential determinants of •NO neuroactivity. Although •NO production is well characterized, the pathways of inactivation *in vivo* remain largely unknown. Here, we characterize the kinetics and the major mechanism of •NO inactivation in the rat brain cortex and hippocampus *in vivo* by measuring locally applied •NO with carbon-fiber microelectrodes (CFMs) and ceramic-based microelectrode arrays (MEAs). An apparent first-order clearance was observed in both brain regions, with decay rate constants (k) of •NO signals of 0.67 to 0.84 per second, significantly higher than the k obtained in agarose gel (0.099 per second), used as a •NO diffusion-control medium. •NO half-life *in vivo*, estimated by mathematical modeling, was 0.42 to 0.75 s. Experiments using MEAs support that the •NO diffusion radius is heterogeneous and related to local metabolic activity and vascular density. After global ischemia, k decreased to control values of diffusion in gel, but during anoxia, k decreased only 21%. Additionally, k in brain slices was threefold to fivefold lower than that *in vivo,* and hemorrhagic shock induced a 53% decrease in k. Overall, the results support that •NO scavenging by circulating erythrocytes constitutes the major •NO-inactivation pathway in the brain. *Antioxid. Redox Signal.* 14, 1011–1021.

Introduction

Nitric oxide (•NO) is an endogenous free radical involved in a variety of physiological functions in the brain, such as learning and memory (46), neuronal development (9), and neurovascular coupling (24). However, •NO has also been implicated in cell-death pathways associated with neurodegenerative disorders (3).

•NO can rapidly diffuse away from its source site across cell membranes, lacks a specific membrane receptor, and can potentially interact with many biologic targets with different kinetics. Thus, •NO effects are critically dependent on its spatiotemporal concentration dynamics and surrounding tissue chemical environment (3, 28). To understand its signaling mechanisms in the brain and develop strategies to modulate its bioactivity in pathologic conditions, it is crucial to know the mechanisms for the regulation of •NO dynamics.

•NO bioactivity depends on the balance between its synthesis and inactivation. It is well established that, in the brain, •NO is synthesized mainly by neuronal •NO synthase via an increase in intracellular Ca^{2+}, after activation of glutamate *N*-methyl-D-aspartate (NMDA) receptors (14). Conversely, the identification of the pathways that govern •NO consumption, imposing on it a short half-life, remains ambiguous, partly because of difficulties in direct •NO measurement in intact tissue. Despite being the major •NO sink in the vasculature (30), the impact of intraerythrocytic hemoglobin (Hb) in brain •NO dynamics remains largely uncertain (21, 29, 30). Conversely, several biologic molecules may contribute in some extent to •NO consumption in brain perivascular tissue, including oxygen (31), cytochrome *c* oxidase (40), superoxide radical (51), a flavo-hemeprotein (13), peroxidases (1), cytochrome-P450 oxidoreductase (18), neuroglobin, and cytoglobin (6, 19). Given this scenario, knowing the relative contribution of perivascular versus vascular •NO inactivation in defining the •NO half-life in the brain is critical to assess the *in vivo* relevance of these mechanisms.

In this study, we addressed this question along with the kinetics and spatial features of subsecond •NO clearance in the rat cerebral cortex and hippocampus *in vivo*, by direct amperometric •NO measurement with carbon-fiber microelectrodes (CFMs) (2) and ceramic-based microelectrode arrays (MEAs) (5). We observed an apparent first-order •NO inactivation, accounting for an estimated •NO half-life of 0.4 to 0.7 s,

[1]Center for Neuroscience and Cell Biology, University of Coimbra, Largo Marquês de Pombal, Coimbra, Portugal.
[2]Department of Anatomy and Neurobiology, Center for Microelectrode Technology, University of Kentucky, Lexington, Kentucky.
[3]Faculty of Pharmacy, Health Sciences Campus, University of Coimbra, Azinhaga de Santa Comba, Coimbra, Portugal.

for physiologically relevant concentrations. In addition, we provide experimental evidence *in vivo* supporting that •NO scavenging by circulating RBCs is the major •NO-inactivation mechanism, shaping •NO-concentration dynamics in the brain. Our findings present new perspectives to understanding the mechanisms involved in the regulation of •NO bioactivity in the CNS, highlighting the importance of the interactions between •NO and the vasculature, with implications in both physiologic and pathologic conditions.

Materials and Methods

Chemicals and solutions

•NO standard solutions were prepared as previously described (2). In brief, purified •NO gas was bubbled for 30 min through deoxygenated phosphate-buffered saline (PBS), 0.05 *M*, pH 7.4. The concentration of •NO saturated solutions was checked by using a ISO-•NOP 2-mm Pt sensor connected to the amperometer ISO-•NO Mark II (World Precision Instruments, Inc., Sarasota, FL), giving an average •NO concentration of 1.70 ± 0.05 m*M* ($n = 9$).

Carbon-fiber microelectrodes fabrication

•NO-selective chemically modified carbon-fiber microelectrodes were fabricated as previously described (45). In brief, single carbon fibers (30 μm; Textron, Lowell, MA) were inserted into borosilicate glass capillaries (1.16 mm i.d. $\times$ 2.0 mm o.d.; Harvard Apparatus Ltd., Boston, MA) and pulled on a vertical puller (Harvard Apparatus). The protruding carbon fibers were cut to obtain an exposed carbon-tip length of 150 to 250 μm. Electrical connection to the carbon fibers was made with silver paste.

Microelectrodes coating

Nafion (Sigma-Aldrich, St. Louis, MO) coating of CFMs and MEAs was done by dipping the microelectrode tip into a fresh Nafion solution (5%) for 1–2 s and drying for 4 min at 170°C. This process was repeated twice. Then CFM tips were electroplated with *ortho*-phenylenediamine (*o*-PD) (Fluka) by applying a potential of +0.7 V versus Ag/AgCl for 30 min, in a 5 m*M* *o*-PD solution. MEAs were electroplated with *meta*-phenylenediamine (*m*-PD) (Sigma-Aldrich) by applying a triangular wave (+0.25 to +0.75; 3 Hz) during 20 min.

Microelectrodes calibration

The system used for all recordings was the Fast Analytical Sensing Technology computer-controlled potentiostat system (FAST-16; Quanteon, Lexington, KY). Measurements were carried out by using constant-voltage amperometry in a two-electrode configuration. The potential of the working microelectrode, for •NO measurement, was +0.9 V versus Ag/AgCl (Bioanalytical Systems; RE-5) when using CFMs and +0.5 V versus Ag/AgCl for MEAs. •NO microelectrode calibrations were performed in the range of 0.4 to 2 μM. Then 100 μM nitrite (Sigma) was added to assess the potential interference from this compound. The selectivity against nitrite, the most relevant interferent in the present study, was $2{,}994 \pm 377$ ($n = 16$) for CFMs and >10,000 ($n = 18$) for MEAs.

For oxygen measurement with CFMs, the applied potential was −0.8 V versus Ag/AgCl. Microelectrodes were calibrated similar to those in previous studies (38), by subtracting the electrochemical current inside brain tissue, after cardiac arrest ($[O_2] = 0$) to the current recorded over the brain surface, superfused with saline ($[O_2] \approx 273\ \mu M$).

Animal and surgical procedures

All animal procedures were approved by the local institutional animal care and use committee and were in accordance with the European Community Council Directive for the Care and Use of Laboratory Animals (86/609/ECC). *In vivo* and *ex vivo* studies were carried out in 8- to 9-week-old Wistar rats (250–390 g), as previously described (2, 5, 22).

Global ischemia by cardiac arrest was induced by a lethal dose of urethane administered intraperitoneally. Cardiac arrest was determined by monitoring the blood flow in the rat rear right paw with a flow probe (Periflux Systems 5010, Perimed, Uppsala, Sweden).

In hypoxia and hyperoxia experiments, a moderate gas flow was created in front of the rat nose by means of a funnel plugged to a gas tank containing nitrogen or 100% oxygen, respectively.

Hemorrhagic shock was induced by withdrawing 6 ml of blood by means of successive 1-ml blood collections via a catheter introduced in the right femoral artery.

Electrochemical Recordings

Micropipette/CFM arrays had a tip separation of 270 to 330 μm. When using MEAs, the micropipette tip was placed between sites 2 and 3, 250 to 300 μm over the recording surface. *In vivo* experiments were carried out in the cerebral cortex and in the CA1 region of the hippocampus (not histologically confirmed). The following coordinates, calculated from bregma, based on the rat brain atlas of Paxinos and Watson (41), were used for CFMs: rat cerebral cortex, anterior-posterior (AP), −3.4; medial-lateral (ML), −2.4; dorsoventral (DV), −1.5; and AP, −4.1; ML, −2.8; DV, −1.5; and for hippocampus, AP, −3.4; ML, −2.4; DV, −2.5; and AP, −4.1; ML, −2.8; DV, −2.5. When using MEAs, micropipette-tip coordinates were cerebral cortex, AP, −3.4; ML, 2.4; DV, −1.4; and AP, −4.1; ML, −2.8; DV, −1.4; and for hippocampus, AP, −3.4; ML, −2.4; DV, −2.7; and AP, −4.1; ML, −2.8; DV, −2.7.

The data-acquisition rate was 10 Hz in CFM experiments and 2 Hz in MEA recordings. After baseline current stabilization (15 min), •NO solutions were pressure ejected from the micropipette by using a Picospritzer III (Parker Hannifin Corp., General Valve Operation). The volume ejected was measured by using a stereomicroscope (Meiji EMZ 13, Tokyo, Japan) fitted with an eyepiece reticule allowing volume measurements with a precision of 2 nl. Usually, different applied volumes were achieved by changing the pressure from 5 to 30 psi or the ejection time from 0.05 to 0.5 s, or both.

For the experiments in agarose gel, a 0.2% (wt/vol) agarose concentration in PBS was used.

Mathematical modeling of •NO diffusion

•NO diffusion from a spherical source was modeled by using Wolfram Mathematica 6.0 software, based on the following equation (42):

$$C_{inst}(a,r,t) = Qe^{-\lambda t}\left[\frac{1}{2}\left(erf\left(\frac{a+r}{2\sqrt{Dt}}\right) + erf\left(\frac{a-r}{2\sqrt{Dt}}\right)\right) - \frac{1}{r}\sqrt{\frac{Dt}{\pi}}\left(\exp\left(\frac{(a-r)^2}{4Dt}\right) - \exp\left(\frac{(a+r)^2}{4Dt}\right)\right)\right] \quad (1)$$

where C is •NO concentration t seconds after an instantaneous burst of •NO production, a is the radius of the sphere, r is the distance between the center of the source sphere and the detector, Q corresponds to the initial •NO concentration at the center of the source, and D is the •NO diffusion coefficient. This model assumes first-order •NO inactivation kinetics, with a first-order decay constant given by λ. Solutions for continuous •NO application were generated by numerically integrating Equation 1 by using the *NIntegrate* command in Wolfram Mathematica 6.0.

Statistical analysis

Kinetic analyses were carried out by using Microcal Origin Pro 7.5. Data are presented as mean ± standard error of the mean (SEM). Differences between two datasets were evaluated with a Student t test. Statistical tests between multiple datasets were carried out by using a one-way analysis of variance (ANOVA).

Results

Nitric oxide signals in agarose gel versus in vivo

We used selective •NO CFMs (45) and the ceramic-based MEAs (44) to understand better the kinetics of •NO clearance in the brain. With CFMs, the clearance rate of exogenously applied •NO *in vivo* in the cerebral cortex and hippocampus was compared with that in agarose gel, which was used to evaluate the contribution of free diffusion to the temporal profile of •NO signals, as previously done with other compounds (39, 47). Fig. 1A shows representative recordings, in which different •NO signal amplitudes were achieved by local application of different volumes of a saturated •NO solution in agarose gel (Fig. 1A, top) and in rat cerebral cortex (Fig. 1A, bottom). The temporal profile of successive •NO signals is very reproducible, regardless of the number and frequency of •NO applications. However, •NO signals *in vivo* are significantly faster than those in agarose. Fig. 1B shows typical normalized •NO signals, which decay with a $t_{1/2}$ of 0.9 s *in vivo* (cortex) versus 7.0 s in agarose. On average, the rise time of signals was 3.90 ± 0.10 s ($n = 15$) from five experiments in agarose and 1.95 ± 0.1 s ($n = 201$) from 16 experiments *in vivo*. Differences in rise time were statistically significant comparing agarose and *in vivo* times ($p < 0.0001$).

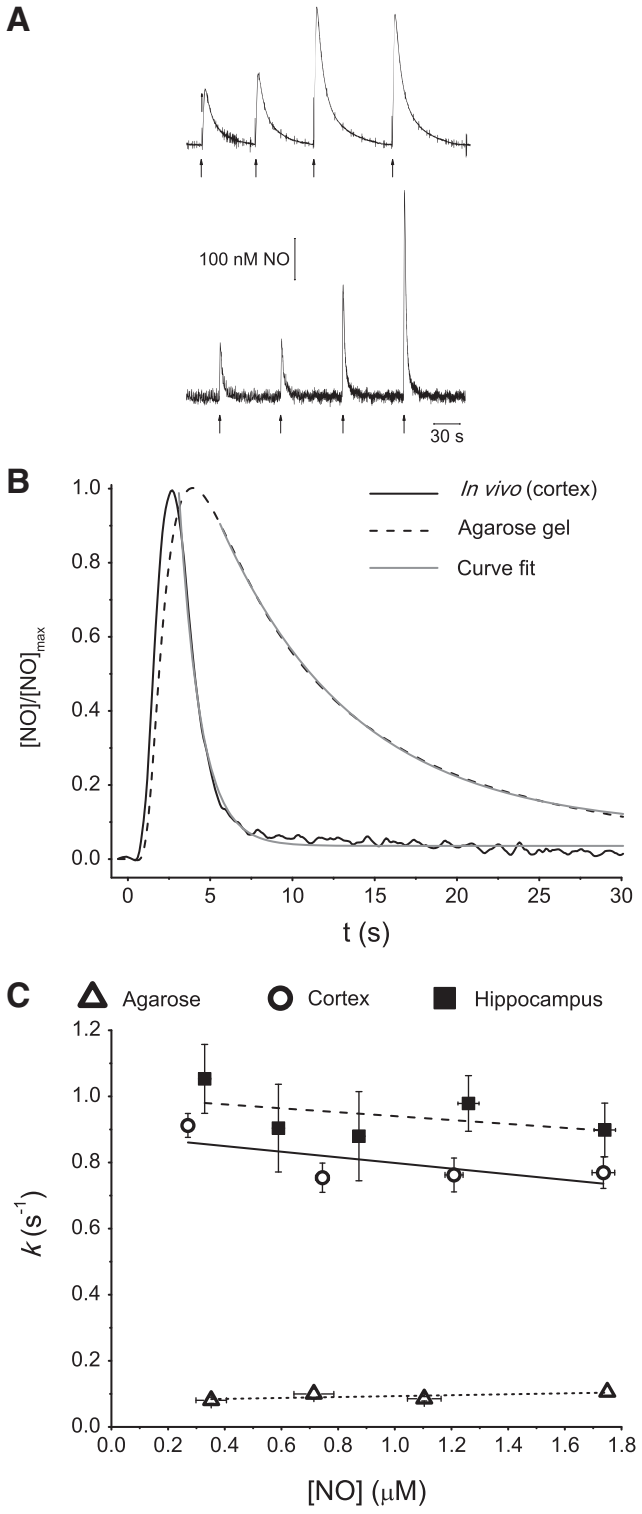

FIG. 1. •NO signals *in vivo* versus agarose gel. (A) Representative signals obtained upon local application of a saturated •NO solution from a micropipette in agarose gel at 37°C *(top)* and *in vivo* in the rat cerebral cortex *(bottom)*. *Arrows* indicate times of •NO application. Volumes applied were 2, 2, 4, and 6 nl in the cortex and <2, <2, 2, and 2 nl in agarose. **(B)** Typical traces showing normalized •NO signals obtained in agarose gel and *in vivo* in rat cerebral cortex. The k values from each first-order decay fit (gray line) were 0.8 per second in rat cerebral cortex and 0.1 per second in agarose. **(C)** The k values as a function of signal amplitude. Data represent an average from eight experiments in cortex and hippocampus and five experiments in agarose. The slope of each linear trend line is not statistically different from zero ($p > 0.05$). Mean k values were 0.83 ± 0.09 per second (mean ± SEM, $n = 8$) in cortex, 0.84 ± 0.1 per second (mean SEM, $n = 8$) in hippocampus, and 0.099 ± 0.006 per second (mean ± SEM, $n = 5$) in agarose.

The kinetics of •NO decay were determined by fitting a first-order exponential decay function to the decay phase of signals, as shown in Fig. 1B. The curve fits are in a good match with signal decay profiles both in agarose and *in vivo*, indicating that the apparent first-order decay rate constant (k) can be used to describe quantitatively the time course of the •NO signal decay. Furthermore, in accordance with apparent first-order decay, k values were constant both *in vivo* and in agarose, for concentrations ranging from 200 to 2,000 nM (Fig. 1C). The mean k was 0.83 ± 0.09 per second ($n = 128$) from eight experiments in cortex, 0.84 ± 0.1 per second ($n = 73$) from eight experiments in hippocampus, and 0.099 ± 0.006 per second ($n = 15$) from five experiments in agarose. The k was significantly higher between both brain regions *in vivo* and in agarose ($p < 0.001$).

•NO scavenging shapes •NO signals

To evaluate whether the temporal profile of •NO signals accurately reflects the kinetics of inactivation reactions in the recording media, we carried out experiments in agarose gel supplemented with the •NO scavenger C-PTIO. Fig. 2A shows the effect of increasing C-PTIO concentrations (10 to 100 μM) on the temporal profile of •NO signals. Both the rise time and the decay rate were affected by the scavenger in a concentration-dependent way. The rise time of signals shown in Fig. 2A decreased from 4.2 s in nonsupplemented agarose to 1 s in agarose supplemented with 100 μM C-PTIO. This result was expected, because the rise time is the instant when the rates of •NO concentration increase because of diffusion from the micropipette and clearance from the recording site become equilibrated. Thus, the higher the clearance rate, the faster this instantaneous equilibrium is attained, which is also in accordance with the lower rise time of •NO signals *in vivo,* as compared with in agarose. By plotting k versus C-PTIO concentration (Fig. 2B), we observed a linear relation with a slope of 0.57×10^4 $M^{-1}s^{-1}$, which is in accordance with the rate constant (0.6×10^4 $M^{-1}s^{-1}$) for the scavenging reaction of •NO by C-PTIO (15), an observation that further accounts for the reliability of the experimental approach. Moreover, the rate constant ($k = 0.70$ per second) obtained in agarose gel supplemented with 100 μM C-PTIO is in the range of the values obtained *in vivo*, supporting the activity of efficient biochemical mechanisms of •NO removal at the recording site *in vivo*.

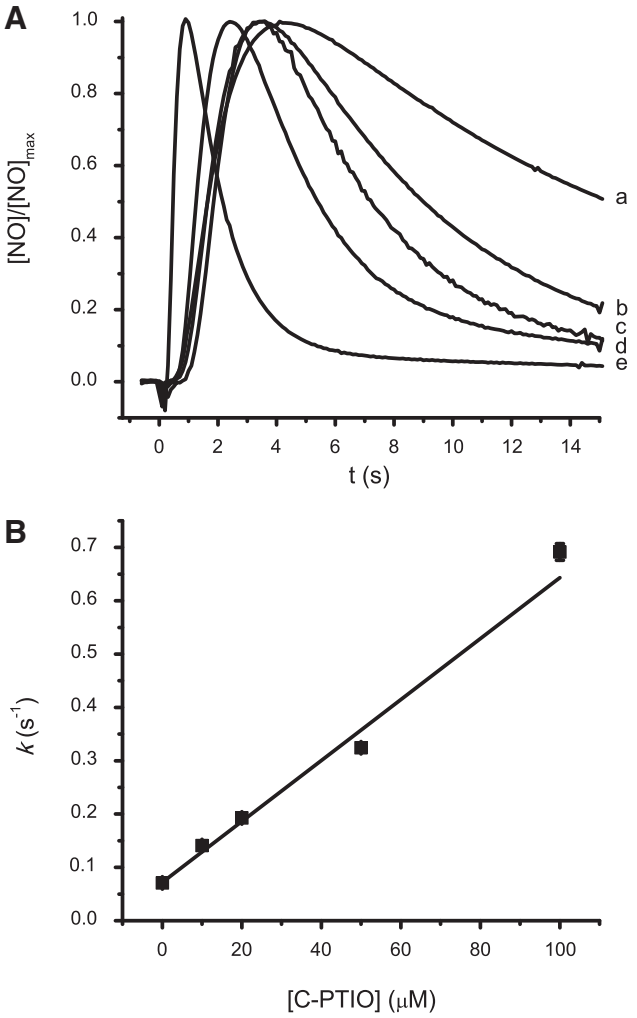

FIG. 2. Effect of •NO scavenging on •NO signals. (A) Temporal profile of normalized •NO signals obtained at 22°C in agarose gel supplemented with C-PTIO. Traces from *a* to *e* were obtained in agarose with 0, 10, 20, 50, and 100 μM C-PTIO, respectively. **(B)** The k values of •NO signals increased linearly with increasing scavenger concentrations with a slope of 0.57×10^4 $M^{-1}s^{-1}$ ($R^2 = 0.975$).

Microelectrode array recordings

MEAs provided spatial resolution of •NO clearance in brain tissue by simultaneously monitoring four brain areas in 200-μm increments in a dorsoventral orientation (Fig. 3A and B). Fig. 3C shows a typical recording obtained on successive local •NO applications in the hippocampus. On average, signal rise time was 2.6 ± 0.2 s ($n = 83$) from 10 experiments in the cortex and 2.2 ± 0.4 s ($n = 64$) from six experiments in the hippocampus ($p > 0.05$). The k values were 0.67 ± 0.06 per second in cortex and 0.77 ± 0.1 per second in hippocampus ($p > 0.05$). Typically, •NO was not detected at all MEA sites, which is not attributable to differences between the LODs of the MEA recording sites. Furthermore, when considering the number of experiments in which •NO was detected from each site, relative to the total number of experiments, it is evident that the sites closer to the micropipette tip (sites 2 and 3) showed the highest probability of •NO detection (Fig. 3D). Comparing sites at the same distance from the •NO source, a greater probability of detecting •NO exists in a more-ventral position in cortex (sites 1 and 2) and in a more-dorsal position in hippocampus (sites 3 and 4). These results suggest a heterogeneous •NO diffusion/inactivation through the tissue microenvironment surrounding MEA sites.

With MEAs, one can also improve the signal-to- noise ratio of •NO signals by subtracting the current of an MEA site that does not detect •NO from an MEA site where •NO is oxidized (Fig. 3C, bottom). With this approach, signals with amplitudes as low as 100 nM were measured. Further to improve the signal-to-noise ratio, a large number of very small signals ($n > 40$) were averaged. Fig. 3E shows k values for low-nanomolar •NO signal amplitudes. The k does not significantly change in this range (ANOVA, $p > 0.05$).

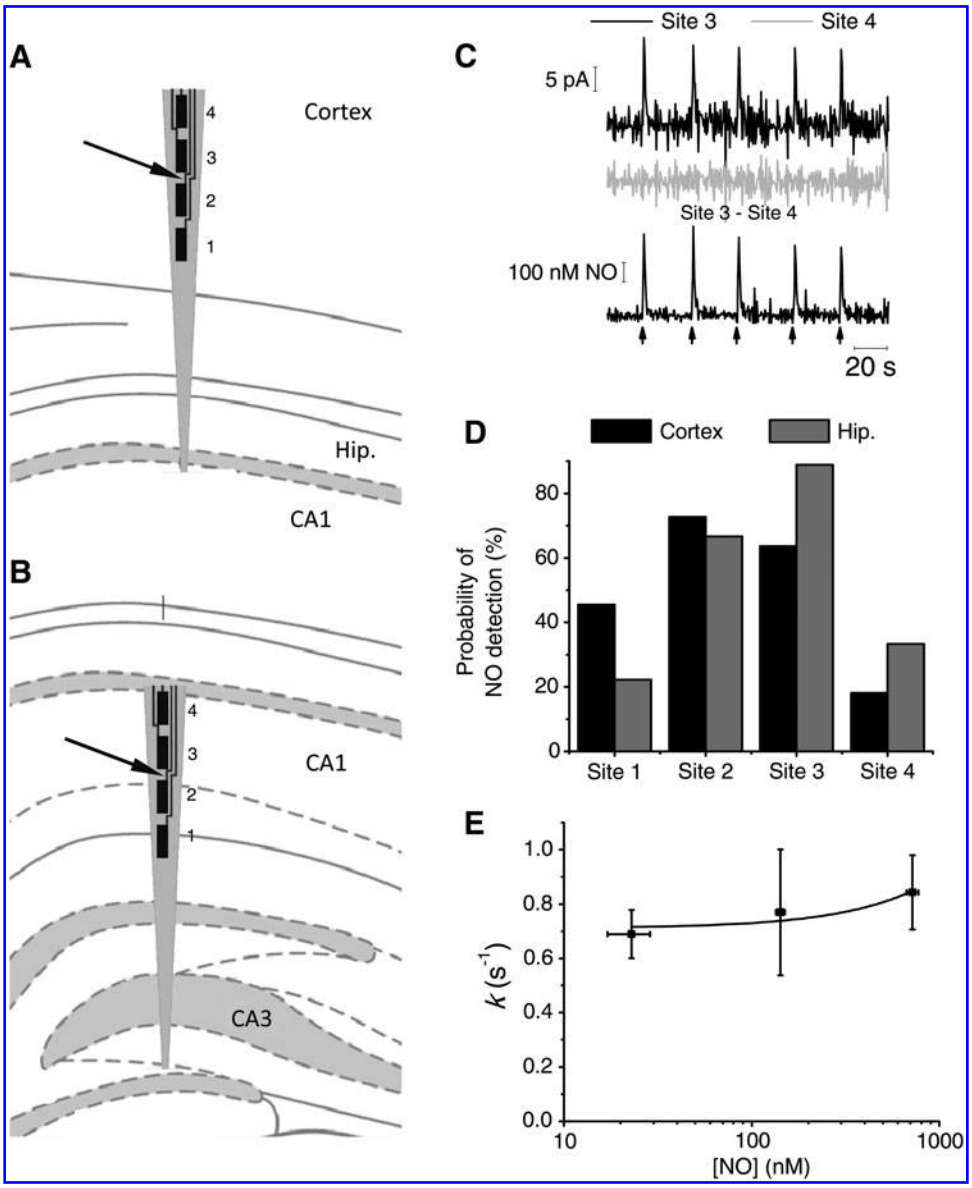

FIG. 3. Recordings with MEAs. The cartoon shows the location of the MEA in the rat brain cortex **(A)** and hippocampus **(B)**, as predicted from the rat brain atlas (41). The numbers 1–4 indentify each MEA site. The micropipette-tip position is indicated by the arrows, 250–300 μm away from the MEA surface **(C,** *top***)**. Representative recording obtained with an MEA on local •NO application from a micropipette in the rat cortex *in vivo*. *Arrows* indicate times of •NO application. Volumes applied were 12.5 nl. **(C,** *bottom***)** Recording obtained by subtracting the current from a site that did not detect •NO (Site 4) from sites that did (Sites 2 and 3). **(D)** Probability of •NO detection in each site in cortex and hippocampus, calculated as the number of experiments in which •NO was detected relative to the total number of experiments ($n = 11$ in cortex and nine in hippocampus). **(E)** Signal k values as a function of signal amplitudes for nanomolar •NO concentrations, *in vivo* ($n = 3$). No significant difference was observed in k between the points shown ($p > 0.05$, ANOVA).

Global ischemia impairs •NO inactivation in vivo

The kinetic data indicate that •NO signals *in vivo* are shaped by a powerful and robust apparent first-order inactivation mechanism. We investigated its potential identity by recording the variation of k after global ischemia (cardiac arrest), induced by a lethal dose of urethane. Fig. 4A shows a representative recording (from seven experiments) of •NO signals *in vivo* and the corresponding k values after urethane administration (Fig. 4C). Fig. 4B illustrates the significant change in •NO signal dynamics shortly after cardiac arrest (Fig. 4B), translating into a decrease in k from 0.73 per second to 0.08 per second and an eightfold increase in signal amplitude. With MEAs, the differences in signal amplitudes between the recording sites *in vivo* greatly decrease after cardiac arrest (Fig. 4D). On average, the ratio of •NO signal amplitudes between sites not detecting/detecting •NO *in vivo* was $56 \pm 15\%$ after cardiac arrest. Together, these results indicate that •NO inactivation is greatly impaired during ischemia.

Oxygen-dependent vs. vascular •NO inactivation

The global ischemia results support that •NO inactivation *in vivo* is an active process, depending either on tissue oxygen supply or on RBC perfusion in cerebral vessels or both. These hypotheses are conceivable, because many •NO-inactivation mechanisms found *in vitro* are oxygen dependent (13, 19, 32, 40). Furthermore, RBCs constitute the strongest •NO sink in the bloodstream (30).

To assess the contribution of oxygen-dependent •NO inactivation, brief hypoxia was induced by exposing the animal to a nitrogen-enriched atmosphere for 1 to 2 min. After the onset of nitrogen exposure, oxygen concentration rapidly decreased in the brain to concentrations less than 10 μM and quickly recovered to baseline levels after nitrogen removal (Fig. 5A). No significant change in k was observed under the same conditions, as compared with control (Fig. 5B), supporting that •NO inactivation is insensitive to moderate decreases in oxygen concentration. Nevertheless, the contribution of •NO-consumption mechanisms with high oxygen

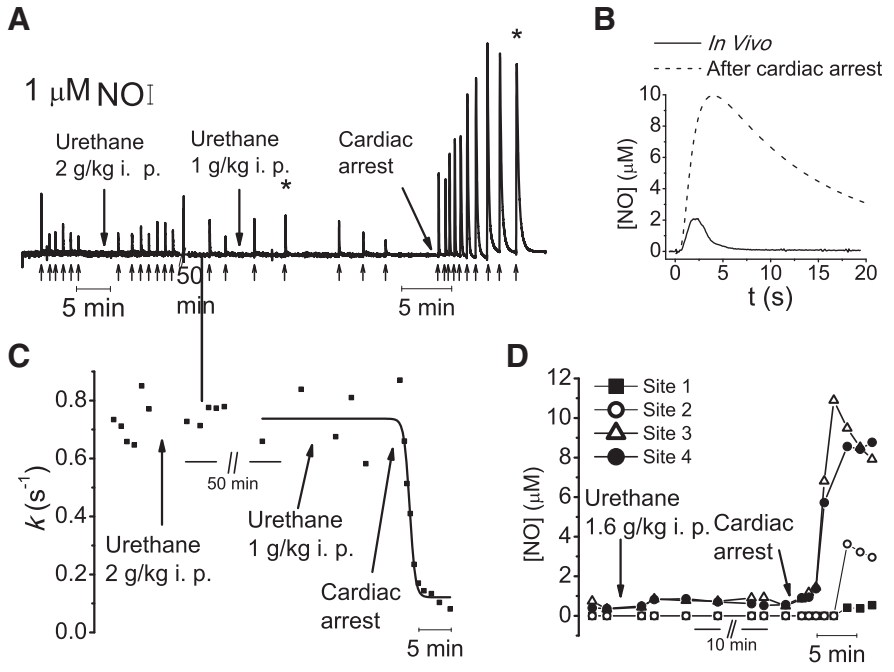

FIG. 4. Global ischemia impairs •NO inactivation. (A) Representative recording of signals from locally applied •NO from a micropipette obtained on cardiac arrest induced by a lethal dose of urethane. Volumes of locally applied •NO solution were 4 nl (*arrows*). The temporal scale of the signals marked with * in **A** is shown in an expanded time scale in **B**. **(C)** The k values of the •NO signals rapidly decreased after cardiac arrest from 0.73 per second to 0.08 per second. **(D)** Representative plot showing the increase in signal amplitudes after cardiac arrest, in different MEA sites. On average, relative amplitudes of MEA sites not detecting/detecting •NO increased from 0 *in vivo* to $56 \pm 15\%$ (mean $\pm$ SEM, $n = 5$) after cardiac arrest.

affinity ($<5\ \mu M$) was still uncertain. Thus, anoxia was induced by nitrite intraperitoneal overdose (200 mg/kg, IP), causing a progressive decrease in oxygen tension in the brain to nearly zero, due to oxidation of a significant fraction of ferrous hemoglobin to metHb (27), resulting in cardiac arrest (Fig. 5C). After nitrite administration, k decreased $21 \pm 5\%$ ($n = 5$) and, after cardiac arrest, further decreased to values similar to those observed in agarose (Fig. 5D).

Despite nitrite oxidation of Hb(II) to Hb(III), which scavenges •NO much more slowly than Hb(II) (10). Lethal levels of

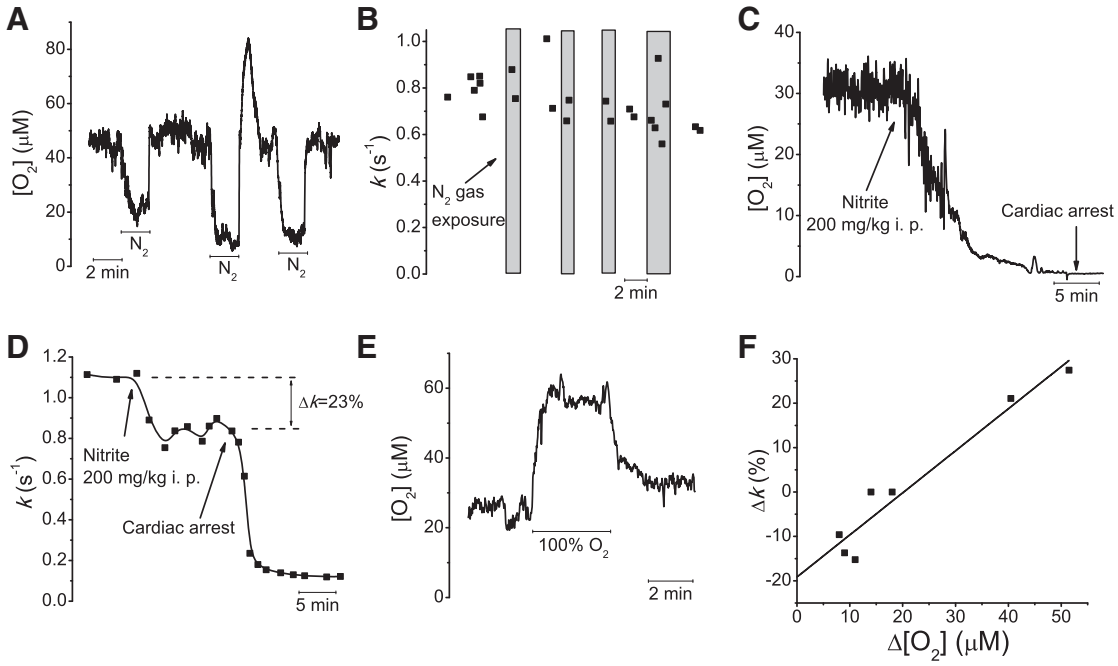

FIG. 5. Oxygen-dependent •NO inactivation. (A) Representative oxygen recording in cortex on successive N_2 exposure periods. **(B)** Under the same conditions, the k for the •NO signals was not significantly affected by hypoxia; $p > 0.05$ ($n = 2$). **(C)** Representative oxygen recording in the hippocampus after nitrite overdose. **(D)** Traces showing that between nitrite administration and cardiac arrest, k decreased $21 \pm 5\%$ (mean $\pm$ SEM, $n = 5$). **(E)** Oxygen recording showing an increase in rat brain-cortex oxygen level during exposure to 100% oxygen gas (hyperoxia). **(F)** Plot showing a linear relation between the increase in local oxygen concentration during hyperoxia (cortex) and the relative change in k values of •NO signals, relative to the normoxic control. The linear regression showed $R^2 = 0.93$; slope, $0.95\%/\mu M$ O_2; and y *intercept* $= -19\%$. Data were obtained from seven experiments in three rats.

metHb are around 70% of total Hb, which should not affect the •NO reaction with RBCs (49), indicating that the decrease observed in k before cardiac arrest is RBC independent. However, other possible nitrite effects, independent of oxygen tension, may contribute to the decrease in k, such as oxidation of plasma free Hb, which can reach 1 μM (21) and hypotension-induced decrease in cerebral blood flow, due to a strong hypoxic vasodilation (26) or decreased cardiac output. Nevertheless, one may conclude that anoxia causes at most a 21% decrease in k.

Further to characterize oxygen-dependent •NO inactivation, we quantified •NO signal decays under conditions of normobaric hyperoxia. For each experiment, both oxygen and •NO recordings were sequentially performed. Hyperoxia-induced brain tissue oxygen concentration increases (Fig. 5E), ranging from 8 to 51 μM. A linear relation was obtained by plotting the variation in oxygen concentration against the relative change in •NO signals k (Fig. 5F). Interestingly, for small oxygen increases (<11 μM), k decreased, whereas high oxygen increases caused an increase in k of about 25%. These variations in k are in accordance with the decreases of 21% during anoxia experiments (where the absolute oxygen change was similar). Together, although these results support the activity of oxygen-dependent •NO-inactivation mechanisms in the brain, the relatively small changes observed in k support that the major mechanism affecting •NO clearance *in vivo* is oxygen independent, pointing to the reaction between •NO and RBCs as the main candidate.

This latter hypothesis was first tested by locally applying •NO in brain slices, a metabolically active brain-tissue preparation devoid of functional vasculature. •NO signals in brain slices, recorded with MEAs, showed an average k of 0.18 ± 0.01 per second both in cortex ($n = 8$) and in hippocampus ($n = 2$). Although these values were significantly higher than the average k of 0.099 per second in agarose ($p < 0.0001$), supporting the activity of •NO-inactivation processes in the brain perivascular tissue, they are more than threefold lower than the average k *in vivo* (Fig. 6A), an observation that further points to the reaction between •NO and RBCs as the major determinant of the regulation of •NO half-life in the brain *in vivo*.

RBC contribution to •NO decay *in vivo* was directly assessed by inducing hemorrhagic shock. With this protocol, the decrease in blood volume causes severe hypotension and ultimately impairs brain microcirculation by decreasing cerebral blood flow and functional capillary density (7). The microcirculation impairment is also supported by the fact that approximately 1 h of progressive blood withdrawal caused cardiac arrest. As shown in Fig. 6B, during hemorrhage, k progressively decreased before cardiac arrest. Although a concomitant decrease in cerebral oxygen tension may have occurred during these experiments, the average decrease in k was $53 \pm 4.6\%$, which is more than twice that during anoxia ($p < 0.01$). Taken together, the results in this section point to a major role of the reaction between •NO and circulating RBCs in governing nitric oxide dynamics in the brain *in vivo*.

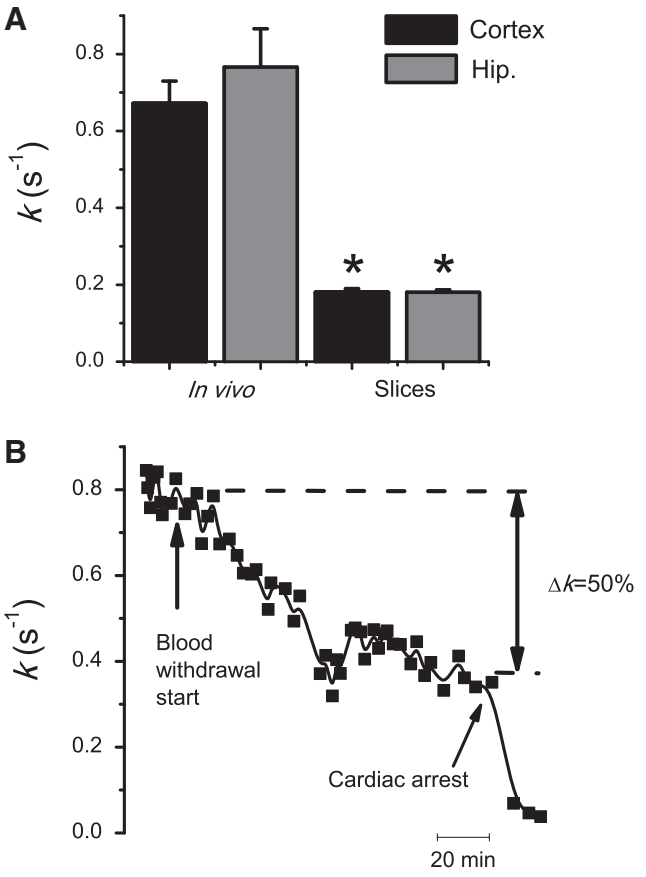

FIG. 6. Vascular •NO inactivation. (A) Bar graph showing that the k *in vivo* was more than threefold higher than that in brain slices (*$p < 0.0001$), recorded by using MEAs. Mean values were 0.67 ± 0.06 per second (mean ± SEM, $n = 10$) in cortex, 0.77 ± 0.1 per second (mean ± SEM, $n = 6$) in hippocampus *in vivo*, and 0.18 ± 0.01 per second (mean ± SEM) in both brain regions in slices ($n = 8$ in cortex; $n = 2$ in hippocampus). **(B)** Graph showing a representative decrease in k after hemorrhagic shock, induced by progressive withdrawal of 6 ml of blood during 40 min. On average, k decreased $53 \pm 5\%$ (mean ± SEM, $n = 3$ experiments), which is significantly higher than that during anoxia ($p < 0.01$).

Modeling •NO diffusion and inactivation

To quantify •NO inactivation, we must take into account the diffusional component of the signals. Reported •NO diffusion coefficients in aqueous solution range from 2.0 to 4.5×10^{-5} cm^2/s (12, 35, 50). However, the assumption that •NO diffusion is not significantly affected by cellular structures was recently disputed by the estimation of a much lower apparent •NO-diffusion coefficient ($D\bullet_{NO}{}^{app}$) of 0.85×10^{-5} cm^2/s across aortic wall tissue (33).

Given the uncertainty regarding $D\bullet_{NO}{}^{app}$ in brain tissue, we estimated the apparent first-order rate constant of •NO inactivation in the brain *in vivo* (λ) by modeling •NO-diffusion/inactivation from the micropipette to the microelectrode, assuming a range of D values (Eq. 1).

Fig. 7A shows the relation between k and λ for D in the range of 1 to 4×10^{-5} cm^2/s, while keeping all the other parameters in Eq. 1 at the values: $a = 112\ \mu$m (a sphere with a volume of 6 nl); $r = 300\ \mu$m; $Q = 1{,}700$ (Q affects the signal amplitude but not the signal shape; we assumed that Q equals the saturated •NO-solution concentration). Taking into account the average k obtained *in vivo* by using CFMs ($k = 0.84$ per second) and the plot in Fig. 7A, the predicted λ as a

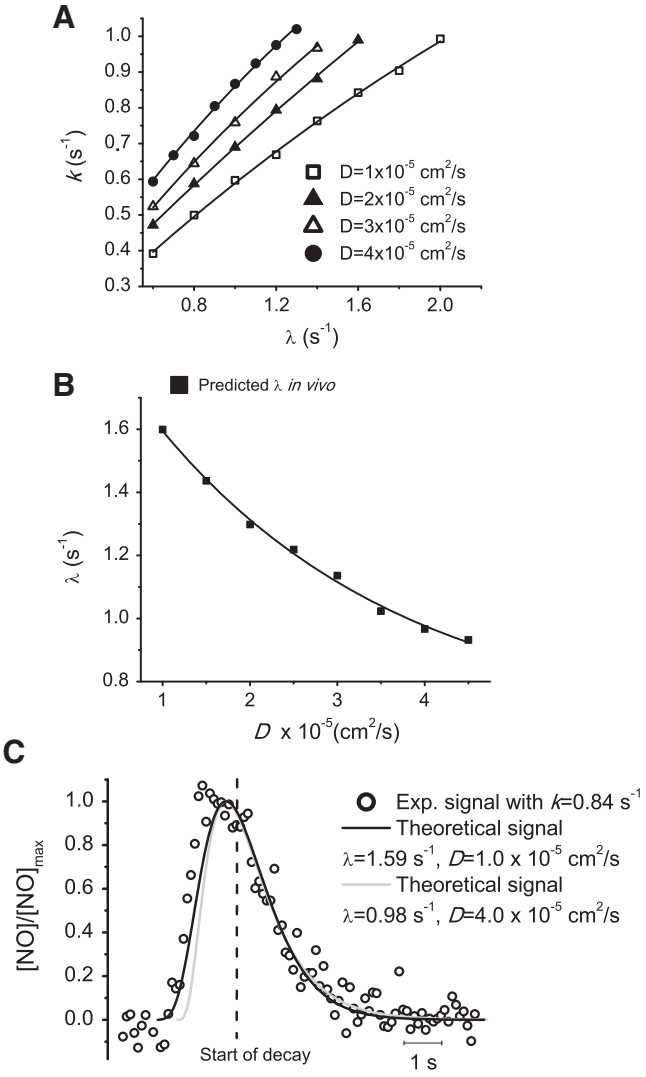

FIG. 7. Mathematical modeling of •NO signals. Unless otherwise stated, the plots were based on Eq. 1, setting Q 1,700 μM; $r = 300\ \mu$m; and $a = 112\ \mu$m. **(A)** Graph of theoretic k values as a function of λ, assuming different D values. Solid lines represent exponential fits. **(B)** Graph showing predicted λ as a function of D, taking into account the mean $k = 0.84$ per second *in vivo* with CFMs and the plot in **(A)**. **(C)** Graph showing representative experimental •NO signal and theoretic signals obtained by using different D values, adjusting λ in accordance with **(B)**. Signals time course was adjusted relative to the beginning of decay.

function of D is shown in Fig. 7B. Based on this relation, a good match between representative experimental and theoretic decay profiles can be obtained by using different D values (Fig. 7C). Considering a range of possible $D\bullet_{NO}{}^{app}$ *in vivo*, from 4.5×10^{-5} to 0.85×10^{-5} cm^2/s, λ would range from 0.92 to 1.64 per second, corresponding to •NO half-lives from 0.75 s to 0.42 s, respectively.

Theoretic signals k was robust to variations in the source volume and application time from 2 to 12 nl and 0 to 0.3 s (<5% variation). Because we estimated λ based on theoretic signals k, this observation accounts for the robustness of our approach.

Discussion

On the basis of experimental data *in vivo* and mathematical modeling, we showed in these studies that •NO scavenging by circulating red blood cells likely constitutes the strongest •NO-inactivation pathway in the rat brain, affecting •NO decay and half-life *in vivo*. This mechanism greatly contributes to a robust apparent first-order kinetics of •NO inactivation, resulting in an estimated •NO half-life of 0.42 to 0.75 s in cortex and hippocampus. It is well established that RBCs are the stronger •NO sink in the vasculature (30). However, the extent to which RBCs can inactivate perivascular •NO has remained unknown and controversial, because of the difficulty in measuring •NO dynamics *in vivo*.

In this study, the observation that global ischemia nearly abolishes •NO inactivation indicated a crucial role of circulating RBCs in supporting •NO inactivation in the brain *in vivo*. Because RBC circulation is tightly coupled with tissue oxygen supply/metabolic activity, we used three different approaches, aiming to isolate the contribution of these factors to •NO inactivation: (a) real-time measurements of •NO changes under anoxia, hypoxia, and hyperoxia; (b) comparison of the kinetics of •NO decay *in vivo* versus brain slices; and (c) measurements under moderately impaired RBC microcirculation *in vivo*. Collectively, the results support a relatively small contribution (<21%) of O_2-dependent •NO inactivation to signal decay and support a major role of •NO scavenging by RBCs in determining •NO half-life in the brain *in vivo*. The continuous flow of RBCs might provide an almost nonsaturable way to inactivate •NO in the brain, which is in agreement with the robust apparent first-order kinetics of •NO clearance observed in our experiments for physiologically relevant •NO signal amplitudes.

In most situations, •NO acts as a paracrine messenger in the brain. After activation of a relatively large brain region, small dispersed •NO sources of low individual efficacy can cooperate to originate an extensive and strong volume signal (43). •NO half-life plays an important role in shaping the resulting volume signal. Mathematical simulations have shown that cooperativity is significantly decreased when assumed •NO half-lives are <500 ms. Conversely, further increases up to 5 s did not considerably increase cooperativity (43). It is noteworthy that our estimated •NO half-life of 0.42 to 0.75 s, by mathematical modeling with a range of $D\bullet_{NO}{}^{app}$ values in the brain from 0.85×10^{-5} cm^2/s to 4.5×10^{-5} cm^2/s, fits in the minimum values needed to ensure strong cooperativity between •NO sources.

Another implication of the estimated •NO half-life is that for endogenous •NO, volume signals with a duration (*i.e.*, a rising and a decay phase) significantly higher than 0.42 to 0.75 s, the temporal encoding of the signal should be mainly controlled by the kinetics of •NO biosynthesis in the tissue. This may constitute an efficient temporal coupling between the integrated nNOS activity of the tissue and the resulting •NO volume signal formed. A recent study from our group (34), in which we have characterized endogenous •NO signals in the rat brain hippocampus following activation of glutamate receptors, indicates that such phenomenon may occur *in vivo* since the endogenous signals had a duration (both the rising and decay phases) about one order of magnitude higher than the estimated •NO half-life in the present study. This observations support that •NO inactivation, in addition to

avoiding the buildup of toxic •NO concentrations, is fine tuned to support efficient •NO volume signaling.

The physiological relevance of finely regulating the levels of excitotoxic compounds in the brain such as •NO and glutamate is evidenced by the similarity between exogenous glutamate and •NO signals (5), which decay much faster than classic neurotransmitters such as DA (44). However, the rapid clearance of glutamate is due to the high-capacity glutamate transporters, primarily located on glia, whose activity can be regulated in different ways in response to a variety of stimuli (11). Our findings on •NO inactivation pose an important question regarding whether the same versatility exists in the regulation of •NO dynamics by the vasculature. Here, we propose biologic processes that might accomplish this task:

1. Vascular density may be envisaged as a long-term mechanism for the regulation of •NO spatiotemporal dynamics. The results with the MEAs support that the vascular density is important in defining the •NO diffusion radius *in vivo.* Based on previous measurements in the brain, the vascular density is higher in the dorsal portion of the cortex in comparison with ventral locations close to the corpus callosum (8). This gradient is inversely related with our probabilities of •NO detection, comparing MEA sites at the same distance from the micropipette tip. Therefore, the different •NO-detection probability distributions among the MEA sites between the brain regions studied are likely due to distinct patterns of vascular density (8). To meet local oxygen demand, vascular density is generally correlated with metabolic activity (20), which often correlates with synaptic activity and •NO production. Therefore, in brain regions with rich •NO signaling, vascular density may be regulated to maintain local physiologic levels of both oxygen and •NO. This hypothesis is further supported by the finding that some regions with similar metabolic activity possess significantly different vascular density, such as the CA1 and CA3 subregions of the hippocampus (8), which may reflect distinct specialization of the local vasculature for the regulation of •NO dynamics, to meet specific •NO-signaling requirements.
2. Short-term regulation of •NO lifetime by vasculature is likely mediated by neurovascular coupling. The transient increase in cerebral blood flow and blood volume after neuronal activation may constitute a feedback mechanism by which synaptically derived •NO increases its own inactivation rate. The physiologic relevance of such a mechanism is uncertain, but it might help protect neurons against unnecessary •NO exposure.
3. To allow •NO-meditated vasodilation, physical barriers exist to limit the rate of the •NO reaction with intraerythrocytic hemoglobin (29, 30, 49). Moreover, experimental evidence supports that •NO likely diffuses more slowly in tissues than in water, and it has been suggested that the •NO diffusion coefficient is dependent on tissue composition (33). Accordingly, it is possible that the vascular wall in blood vessels retards •NO diffusion from brain parenchyma to the bloodstream and, in this way, limits the vascular •NO-inactivation rate in the brain. In this case, regulation of •NO diffusion through vascular walls may constitute a mechanism for the modulation of •NO half-life in the brain. Further experiments are needed to clarify the biologic meaning of interactions between •NO and the vasculature, but given the importance of RBCs in •NO inactivation, shown in this work, these processes might be crucial in the regulation of brain •NO signaling.

In pathologic situations affecting these mechanisms, a deregulation of •NO levels may occur, such as in ischemia/reperfusion. We observed a great decrease in the •NO-inactivation rate during ischemia, which might potentiate •NO accumulation in the affected tissue, formed from either residual NOS activity or NOS-independent •NO-synthesis mechanisms, such as nitrite ischemic reduction (25). It has been found that preischemic administration of •NO donors or nitrite *in vivo* decreases brain ischemia/reperfusion infarct volume in models of focal ischemia (25). One of the mechanisms underlying a neuroprotective role of •NO during ischemia is its vasodilatory action, which likely enhances microcirculation in the regions adjacent to the affected area (penumbra). Thus, it is possible that the impairment of •NO inactivation in the brain region affected by ischemia is protective by increasing local •NO availability and consequently enhancing microcirculation in the adjacent tissue, contributing to the decrease the infarct volume. After reperfusion, impairment of brain microcirculation also has been observed (23). However, in this phase, significant redox alterations also occur in the tissue, which may change the •NO-inactivation rate independent of RBCs. Other pathologies with recognized impairment of cerebral vasculature are multiple sclerosis and Alzheimer disease (36, 37). Our findings provide new perspectives for understanding •NO signaling alterations in these diseases.

Apart from •NO scavenging by circulating RBCs, the results in brain slices also support the activity of perivascular •NO inactivation. Interestingly, the decrease in k observed *in vivo* during anoxia (21%) is similar to the difference between k in brain slices and agarose, relative to the average k *in vivo* (15%), supporting that inactivation mechanisms impaired during anoxia *in vivo* are active in brain slices. Oxygen-dependent •NO inactivation was also supported by hyperoxia experiments, in which a maximum k increase of 25% was observed for oxygen increases of $\sim 45\,\mu M$. These results support a nonsaturable trend in oxygen-dependent •NO inactivation and support that it is, at least in part, not mediated by a high oxygen-affinity mechanism. Another interesting point is that the decrease in k for small oxygen increases, supporting a combined effect of two processes with opposite effects in k during hyperoxia: a decrease in cerebral blood flow, due to hyperoxic vasoconstriction (48) and the increase in tissue oxygen content. The linear trend line *y intercept* in Fig. 5F of −19% might give an estimation of the isolated effect of vasoconstriction in •NO-signal k values. However, it is unclear whether the contribution of vasoconstriction was constant along the whole range of O_2 increases obtained.

Oxygen-dependent •NO inactivation has been frequently found in dispersed preparations *in vitro*, resulting from the activity of molecules such as globins, some ubiquitous detoxifying enzymes, and cytochrome *c* oxidase (13, 18, 19, 40). In intact brain tissue, an unknown mechanism imposing a •NO half-life of 10 ms, for •NO concentrations <10 nM, has

been reported in acute cerebellar slices (17), 60-fold slower in organotypic cerebellar slices (16). These half-lives are significantly lower than we found in brain slices of cortex and hippocampus, which may suggest significant heterogeneity in perivascular •NO inactivation among different brain regions. However, further experiments are needed to confirm this hypothesis, because the previous studies were based on the measurement of cGMP accumulation in tissue.

Our results indicate that, at the tissue level, the •NO-consuming activity of brain perivascular tissue is much weaker than that of the vasculature. However, intraneuronal •NO inactivation may serve as an additional barrier to protect vital intracellular structures against •NO toxicity (4) or even finely to regulate intracellular •NO effects, as recently proposed for cytoglobin in vascular cells (19).

In summary, this study evidences a critical role of the vasculature in the regulation of •NO spatiotemporal dynamics in the brain. We showed that the magnitude of •NO inactivation attributable to the vasculature is much higher than perivascular •NO inactivation. This study helps clarify what contributes to •NO inactivation, which previously remained largely unknown, having implications for the understanding of •NO signaling in the brain in either normal physiologic or pathologic situations and shows that caution should be taken when extrapolating conclusions regarding •NO dynamics from *in vitro* studies to physiological situations. Finally, our results support that new therapeutic approaches targeting cerebral vasculature might be developed to regulate •NO levels in pathologic situations.

Acknowledgments

This work was partially supported by grant SAU-BEB/103228/2008 from FCT(Portugal) and Calouste Gulbenkian Foundation (Prémio Estímulo à Investigação 2008). RMS and CFL acknowledge FCT fellowships SFRH/BD/31051/2006 and SFRH/BD/27333/2006, respectively. We thank Dr. Jorge Quintero from the Center for Microelectrode Technology, University of Kentucky, for his work on the brain-slice preparations.

Author Disclosure Statement

No competing financial interests exist.

References

1. Abu-Soud HM, Hazen SL. Nitric oxide is a physiological substrate for mammalian peroxidases. *J Biol Chem* 275: 37524–37532, 2000.
2. Barbosa RM, Lourenco CF, Santos RM, Pomerleau F, Huettl P, Gerhardt GA, and Laranjinha J. In vivo real-time measurement of nitric oxide in anesthetized rat brain. *Methods Enzymol* 441: 351–367, 2008.
3. Brune B. Nitric oxide: a short lived molecule stays alive. *Pharmacol Res* 25: 421–426, 2009.
4. Brunori M and Vallone B. Neuroglobin, seven years after. *Cell Mol Life Sci* 64: 1259–1268, 2007.
5. Burmeister JJ, Pomerleau F, Palmer M, Day BK, Huettl P, and Gerhardt GA. Improved ceramic-based multisite microelectrode for rapid measurements of L-glutamate in the CNS. *J Neurosci Methods* 119: 163–171, 2002.
6. Burmester T, Weich B, Reinhardt S, and Hankeln T. A vertebrate globin expressed in the brain. *Nature* 407: 520–523, 2000.
7. Cabrales P, Tsai AG, and Intaglietta M. Is resuscitation from hemorrhagic shock limited by blood oxygen-carrying capacity or blood viscosity? *Shock* 27: 380–389, 2007.
8. Cavaglia M, Dombrowski SM, Drazba J, Vasanji A, Bokesch PM, and Janigro D. Regional variation in brain capillary density and vascular response to ischemia. *Brain Res* 910: 81–93, 2001.
9. Contestabile A and Ciani E. Role of nitric oxide in the regulation of neuronal proliferation, survival and differentiation. *Neurochem Int* 45: 903–914, 2004.
10. Cooper CE. Nitric oxide and iron proteins. *Biochim Biophys Acta* 1411: 290–309, 1999.
11. Danbolt NC. Glutamate uptake. *Prog Neurobiol* 65: 1–105, 2001.
12. Denicola A, Souza JM, Radi R, and Lissi E. Nitric oxide diffusion in membranes determined by fluorescence quenching. *Arch Biochem Biophys* 328: 208–212, 1996.
13. Gardner PR, Martin LA, Hall D, and Gardner AM. Dioxygen-dependent metabolism of nitric oxide in mammalian cells. *Free Radic Biol Med* 31: 191–204, 2001.
14. Garthwaite J and Boulton CL. Nitric oxide signaling in the central nervous system. *Annu Rev Physiol* 57: 683–706, 1995.
15. Goldstein S, Russo A, and Samuni A. Reactions of PTIO and carboxy-PTIO with *NO, *NO2, and O2-*. *J Biol Chem* 278: 50949–50955, 2003.
16. Hall CN and Attwell D. Assessing the physiological concentration and targets of nitric oxide in brain tissue. *J Physiol* 586: 3597–3615, 2008.
17. Hall CN and Garthwaite J. Inactivation of nitric oxide by rat cerebellar slices. *J Physiol* 577: 549–567, 2006.
18. Hall CN, Keynes RG, and Garthwaite J. Cytochrome P450 oxidoreductase participates in nitric oxide consumption by rat brain. *Biochem J* 419: 411–418, 2009.
19. Halligan KE, Jourd'heuil FL, and Jourd'heuil D. Cytoglobin is expressed in the vasculature and regulates cell respiration and proliferation via nitric oxide dioxygenation. *J Biol Chem* 284: 8539–8547, 2009.
20. Harder DR, Zhang C, and Gebremedhin D. Astrocytes function in matching blood flow to metabolic activity. *News Physiol Sci* 17: 27–31, 2002.
21. Hobbs AJ, Gladwin MT, Patel RP, Williams DL, and Butler AR. Haemoglobin: NO transporter, NO inactivator or NOne of the above? *Trends Pharmacol Sci* 23: 406–411, 2002.
22. Hoffman AF and Gerhardt GA. Differences in pharmacological properties of dopamine release between the substantia nigra and striatum: an in vivo electrochemical study. *J Pharmacol Exp Ther* 289: 455–463, 1999.
23. Hossmann KA. Reperfusion of the brain after global ischemia: hemodynamic disturbances. *Shock* 8: 95–101; discussion 102–103, 1997.
24. Iadecola C. Regulation of the cerebral microcirculation during neural activity: is nitric oxide the missing link? *Trends Neurosci* 16: 206–214, 1993.
25. Jung KH, Chu K, Ko SY, Lee ST, Sinn DI, Park DK, Kim JM, Song EC, Kim M, and Roh JK. Early intravenous infusion of sodium nitrite protects brain against in vivo ischemia-reperfusion injury. *Stroke* 37: 2744–2750, 2006.
26. Kim-Shapiro DB, Gladwin MT, Patel RP, and Hogg N. The reaction between nitrite and hemoglobin: the role of nitrite in hemoglobin-mediated hypoxic vasodilation. *J Inorg Biochem* 99: 237–246, 2005.
27. Kohn MC, Melnick RL, Ye F, and Portier CJ. Pharmacokinetics of sodium nitrite-induced methemoglobinemia in the rat. *Drug Metab Dispos* 30: 676–683, 2002.

28. Ledo A, Frade J, Barbosa RM, and Laranjinha J. Nitric oxide in brain: diffusion, targets and concentration dynamics in hippocampal subregions. *Mol Aspects Med* 25: 75–89, 2004.
29. Liao JC, Hein TW, Vaughn MW, Huang KT, and Kuo L. Intravascular flow decreases erythrocyte consumption of nitric oxide. *Proc Natl Acad Sci U S A* 96: 8757–8761, 1999.
30. Liu X, Miller MJ, Joshi MS, Sadowska-Krowicka H, Clark DA, and Lancaster JR Jr. Diffusion-limited reaction of free nitric oxide with erythrocytes. *J Biol Chem* 273: 18709–18713, 1998.
31. Liu X, Miller MJ, Joshi MS, Thomas DD, Lancaster JR, Jr. Accelerated reaction of nitric oxide with O_2 within the hydrophobic interior of biological membranes. *Proc Natl Acad Sci U S A* 95: 2175–2179, 1998.
32. Liu X, Srinivasan P, Collard E, Grajdeanu P, Lok K, Boyle SE, Friedman A, and Zweier JL. Oxygen regulates the effective diffusion distance of nitric oxide in the aortic wall. *Free Radic Biol Med* 48: 554–559, 2005.
33. Liu X, Srinivasan P, Collard E, Grajdeanu P, Zweier JL, and Friedman A. Nitric oxide diffusion rate is reduced in the aortic wall. *Biophys J* 94: 1880–1889, 2008.
34. Lourenco CF, Santos R, Barbosa RM, Gerhardt G, Cadenas E, and Laranjinha J. In vivo modulation of nitric oxide concentration dynamics upon glutamatergic neuronal activation in the hippocampus. *Hippocampus* [Epub ahead of print]; doi:10.1002/hipo.20774
35. Malinski T, Taha Z, Grunfeld S, Patton S, Kapturczak M, and Tomboulian P. Diffusion of nitric oxide in the aorta wall monitored in situ by porphyrinic microsensors. *Biochem Biophys Res Commun* 193: 1076–1082, 1993.
36. Meyer EP, Ulmann-Schuler A, Staufenbiel M, and Krucker T. Altered morphology and 3D architecture of brain vasculature in a mouse model for Alzheimer's disease. *Proc Natl Acad Sci U S A* 105: 3587–35892, 2008.
37. Minagar A and Alexander JS. Blood-brain barrier disruption in multiple sclerosis. *Mult Scler* 9: 540–549, 2003.
38. Nair PK, Buerk DG, and Halsey JH Jr. Comparisons of oxygen metabolism and tissue PO2 in cortex and hippocampus of gerbil brain. *Stroke* 18: 616–622, 1987.
39. Nicholson C and Sykova E. Extracellular space structure revealed by diffusion analysis. *Trends Neurosci* 21: 207–215, 1998.
40. Palacios-Callender M, Hollis V, Mitchison M, Frakich N, Unitt D, and Moncada S. Cytochrome c oxidase regulates endogenous nitric oxide availability in respiring cells: a possible explanation for hypoxic vasodilation. *Proc Natl Acad Sci U S A* 104: 18508–18513, 2007.
41. Paxinos C and Watson G. *The Rat Brain in Stereotaxic Coordinates.* New York: Academic Press, 2007.
42. Philippides A, Husbands P, and O'Shea M. Four-dimensional neuronal signaling by nitric oxide: a computational analysis. *J Neurosci* 20: 1199–1207, 2000.
43. Philippides A, Ott SR, Husbands P, Lovick TA, and O'Shea M. Modeling cooperative volume signaling in a plexus of nitric-oxide-synthase-expressing neurons. *J Neurosci* 25: 6520–6532, 2005.
44. Sabeti J, Adams CE, Burmeister J, Gerhardt GA, and Zahniser NR. Kinetic analysis of striatal clearance of exogenous dopamine recorded by chronoamperometry in freely moving rats. *J Neurosci Methods* 121: 41–52, 2002.
45. Santos RM, Lourenco CF, Piedade AP, Andrews R, Pomerleau F, Huettl P, Gerhardt GA, Laranjinha J, and Barbosa RM. A comparative study of carbon fiber-based microelectrodes for the measurement of nitric oxide in brain tissue. *Biosens Bioelectron* 24: 704–709, 2008.
46. Susswein AJ, Katzoff A, Miller N, and Hurwitz I. Nitric oxide and memory. *Neuroscientist* 10: 153–162, 2004.
47. Tao L and Nicholson C. Diffusion of albumins in rat cortical slices and relevance to volume transmission. *Neuroscience* 75: 839–847, 1996.
48. Tsai AG, Cabrales P, Winslow RM, and Intaglietta M. Microvascular oxygen distribution in awake hamster window chamber model during hyperoxia. *Am J Physiol Heart Circ Physiol* 285: H1537–H1545, 2003.
49. Vaughn MW, Huang KT, Kuo L, and Liao JC. Erythrocytes possess an intrinsic barrier to nitric oxide consumption. *J Biol Chem* 275: 2342–2348, 2000.
50. Zacharia IG and Deen WM. Diffusivity and solubility of nitric oxide in water and saline. *Ann Biomed Eng* 33: 214–222, 2005.
51. Zhilyaev SY, Moskvin AN, Platonova TF, Gutsaeva DR, Churilina IV, and Demchenko IT. Hyperoxic vasoconstriction in the brain is mediated by inactivation of nitric oxide by superoxide anions. *Neurosci Behav Physiol* 33: 783–787, 2003.

Address correspondence to:
Rui M. Barbosa
Faculty of Pharmacy
Health Sciences Campus
University of Coimbra
Azinhaga de Santa Comba
3000-548, Coimbra
Portugal

E-mail: rbarbosa@ff.uc.pt

Date of first submission to ARS Central, May 12, 2010; date of final revised submission, July 13, 2010; date of acceptance, August 13, 2010.

Abbreviations Used

CA1 = cornus ammonis 1
C-PTIO = 2-(4-carboxyphenyl)-4,4,5,5-tetramethylimidazoline-1-oxyl-3-oxide;
DA = dopamine
Hb = hemoglobin
o-PD = *o*-phenylenediamine
PBS = phosphate-buffered saline
RBCs = red blood cells

This article has been cited by:

1. João Laranjinha, Ricardo M. Santos, Cátia F. Lourenço, Ana Ledo, Rui M. Barbosa. 2012. Nitric oxide signaling in the brain: translation of dynamics into respiration control and neurovascular coupling. *Annals of the New York Academy of Sciences* **1259**:1, 10-18. [CrossRef]
2. Ricardo M. Santos, Cátia F. Lourenço, Ana Ledo, Rui M. Barbosa, João Laranjinha. 2012. Nitric Oxide Inactivation Mechanisms in the Brain: Role in Bioenergetics and Neurodegeneration. *International Journal of Cell Biology* **2012**, 1-13. [CrossRef]
3. Ricardo M. Santos, Cátia F. Lourenço, Greg A. Gerhardt, Enrique Cadenas, João Laranjinha, Rui M. Barbosa. 2011. Evidence for a pathway that facilitates nitric oxide diffusion in the brain. *Neurochemistry International* **59**:1, 90-96. [CrossRef]